



CrossMark
 click for updates

Cite this: *RSC Adv.*, 2015, 5, 85196

Effect of size and oxidation state of platinum nanoparticles on the electrocatalytic performance of graphene-nanoparticle composites†

Avijit Mondal and Nikhil R. Jana*

A surfactant and stabilizer free graphene-based composite with Pt nanoparticles is considered to be a promising electrocatalyst with greatly improved performance. Here we show that both the size and oxidation state of Pt nanoparticles can significantly influence the electrocatalytic performance of the nanocomposite. We have synthesized Pt-graphene nanocomposites with varied sizes and oxidation states of Pt nanoparticles and test their catalytic activity towards methanol electro-oxidation. We found that the size <1.5 nm with mixed oxidation offers methanol oxidation at lower onset potential and with better tolerance to CO poisoning. However, these benefits are lost due to catalyst durability and thus catalytic current decays rapidly with time. As the nanoparticle size increases in the range of 2–5 nm this onset potential increases, CO tolerance decreases but the catalytic current becomes more stable with time. Thus an optimum nanoparticle size of 2.2 nm shows the best catalytic activity and durability. The oxygenic platinum with variable oxidation states offers stable grafting with the graphene surface, prevents active Pt (0) sites and assists for better CO tolerance. This result would be useful in the design and development of electrocatalysts with better performances.

Received 24th August 2015
 Accepted 25th September 2015

DOI: 10.1039/c5ra17087g

www.rsc.org/advances

1. Introduction

Graphene based composites with metal nanoparticles have been widely used in fuel cell catalysis, photocatalysis and catalytic organic transformation.^{1–3} A variety of noble metals such as Pt, Pd, Au and their alloys have been used as electrocatalysts for the oxidation of methanol, formic acid, ethanol and oxygen reduction reaction.^{4–8} It is reported that graphene offers an ideal catalyst support due to the outstanding mechanical strength, chemical and thermal stability, high surface area and high conductivity.⁹ The electrocatalytic performance of these graphene-based nanocomposites depends on the nature of the metal, size of the nanoparticles, loading of nanoparticles and stability of the nanocomposite. It is reported that smaller size of nanoparticle can greatly improve the catalytic performance.^{8,10,11} However, catalytic current decreases with time due to stability issues of composite and nanoparticles either aggregate or detach from composite.¹² In addition presence of surfactant and polymer stabilizer (that are used for nanocomposite synthesis) can severely limit the catalytic

performance by lowering the accessibility of surface metal atoms.¹³

One significant advantage of graphene as a solid support is that it can stabilize ultra-small nanoparticles as well as provides accessibility of nanoparticle surface to reactants.^{12,14–17} However, commonly used synthesis approach involves physical or chemical linking between graphene and nanoparticle *via* hydrophobic interaction, electrostatic interaction or covalent bonding and in most cases additional linker molecule/surfactant/polymer are used to stabilize the nanocomposite.^{7,18–20} We have recently shown that surfactant free metal-graphene nanocomposite can be prepared by reacting partially reduced colloidal graphene oxide with the respective colloidal metal oxide/hydroxide and they can be used as high performance electrocatalyst.²¹ This approach produces Pt-graphene nanocomposite which is composed of highly dispersed Pt-Pt^{II}-Pt^{IV} based nanoparticle of 2.2 nm size and produces high and stable catalytic current for ethanol and formic acid oxidation. This size of Pt nanoparticle is smaller than conventionally used colloid-chemical routes^{12,18,22} along with mixed oxidation states and thus produced better performance. However, effect of further reduction of size of Pt nanoparticle and effect of nanoparticle size is not studied. Earlier reports demonstrate the particle size effect and shows that atomic layer or subnanometer Pt clusters or smaller Pt nanoparticles can produce even better catalytic current but the catalytic current is shown to decay rapidly with time.^{23,24}

Centre for Advanced Materials, Indian Association for the Cultivation of Science, Jadavpur, Kolkata-700032, India. E-mail: camrj@iacs.res.in; Fax: +91-33-24732805; Tel: +91-33-24734971

† Electronic supplementary information (ESI) available: Details of characterization of nanocomposites, electrocatalytic oxidation of methanol by nanocomposites with Pt nanoparticle size of 0.95 nm, 1.5 nm and 2.0 nm and electrochemically active surface area measurement for three nanocomposites. See DOI: 10.1039/c5ra17087g

Here we have studied both the effect of Pt nanoparticle size as well as oxidation state on the electrochemical performance of Pt-graphene nanocomposite. We have synthesized different Pt-graphene nanocomposites with varied Pt nanoparticle size from 1–5 nm and test their catalytic activity towards methanol electro-oxidation under acidic condition. Methanol electro-oxidation is selected because the direct methanol fuel cells is considered as most attractive among various fuel cell technologies due to high energy density, high efficiency, low cost and eco-friendly nature.^{25–27} It is found that the Pt is the most effective one and playing important role to achieve faster kinetics of anodic reaction of methanol electro oxidation.²⁸ We found that Pt nanoparticle of <1.5 nm size with mixed oxidation state offers the advantage of lower onset potential of methanol oxidation and better tolerance to CO poisoning but these benefits are lost with repeated electrochemical cycle due to poor durability of catalyst. As the nanoparticle size increases to 2.2 nm the onset potential of methanol oxidation is increased and CO tolerance is decreased but offers higher catalytic current and better current stability. Further increase of particle size lowers the catalytic performance due to higher onset oxidation potential, lower CO tolerance and poor current stability. The oxygenic platinum with variable oxidation state offers stable grafting with graphene surface, prevents active Pt (0) sites during repeated cycles and facilitate conversion of CO to CO₂. This study shows the role of Pt nanoparticle size and oxidation state in the electrochemical performance of nanocomposites and would help in designing electrocatalyst with better performance.

2. Experimental section

2.1 Materials and reagents

Graphite powder (<20 μm), hydrazine monohydrate (98%), hexachloroplatinic acid hexahydrate (H₂PtCl₆ · 6H₂O) and Pt on graphitized carbon (Pt/C, 20 wt%) were purchased from Sigma-Aldrich and used as received. Methanol and sulphuric acid (98%) were purchased from Merck, India. All other reagents were of analytical grade and used without further purification. All the solutions were prepared by using double-distilled water.

2.2 Synthesis of partially reduced graphene oxide

Graphene oxide was prepared by modified Hummer's method²⁹ and stock solution was made with concentration of ~1.5 mg mL⁻¹. Next, ~20 μL of hydrazine was added to 1.2 mL of graphene oxide solution and heated at 80–90 °C with constant stirring for 45 minutes.²¹ Resultant partially reduced graphene oxide was purified by adding 100 μL of NaCl solution (160 mg mL⁻¹) followed by centrifugation and repeated washing of precipitate with pure water to remove any free reagents. The residue was redispersed in 1.2 mL distilled water by ultrasonication.

2.3 Preparation of PtGN-1

In a vial 1.5 mL of H₂PtCl₆ solution (10 mM) was mixed with 30–50 μL NaOH solution (1 M). Next, 400 μL of this freshly

prepared basic platinum salt solution was mixed with 1.2 mL of colloidal solution of partially reduced graphene oxide. The mixture was kept under constant stirring for 12–24 h to prepare different PtGN nanocomposites. The PtGN-1 was prepared with 18 h incubation. Other two PtGN nanocomposites were prepared with 12 h and 24 h incubation. If the basic Pt salt solution is reacted with reduced graphene oxide for 12 h then PtGN is formed with the Pt size of 0.95 nm. If reacted for 18 h then PtGN-1 with Pt nanoparticle of 1.5 nm is formed. If reacted throughout 24 h then PtGN with Pt nanoparticle of 2 nm is formed. Resultant PtGN-1 was separated by centrifuge and then dispersed in fresh water. This separation–redispersion was repeated for 3–4 times and finally PtGN-1 was dispersed in fresh water for further experiments.

2.4 Preparation of PtGN-2

In this case 1.5 mL of H₂PtCl₆ solution (10 mM) was mixed with 30–50 μL NaOH solution (1 M) and kept undisturbed for 1–2 days at room temperature. This allows the formation of colloidal platinum oxide nanocrystals.^{30,31} Next, 400 μL of this colloidal platinum oxide solution was added to 1.2 mL of colloidal solution of partially reduced graphene oxide and kept under stirring for 7–8 h. Resultant PtGN-2 was separated by centrifuge and then dispersed in fresh water. This separation–redispersion was repeated for 3–4 times and finally PtGN-2 was dispersed in fresh water for further experiments.

2.5 Preparation of PtGN-3

In this case 400 μL H₂PtCl₆ (10 mM) was mixed with 1.2 mL of partially reduced graphene oxide solution. Next, 200 μL sodium borohydride solution (5 mg mL⁻¹) was added and stirred for one hour. Resultant PtGN-3 was centrifuged and washed several times with pure water. The final products were dispersed in 400 μL water *via* ultrasonication.

2.6 Materials characterization

Transmission electron microscopic (TEM) samples were prepared by putting a drop of particle dispersion on carbon coated copper grid and observed under FEI Tecnai G2 F20 microscope. Raman spectra were recorded using Agiltron R3000 Raman spectrometer with 785 nm excitation laser and X-ray photoelectron spectroscopy was performed using Omicron (Serial No. 0571) X-ray photoelectron spectrometer. Amount of metal present in the composite materials was measured by Optima 2100 DV (Perkin Elmer) inductively coupled plasma atomic emission spectroscopy (ICP-AES).

2.7 Electrochemical measurements

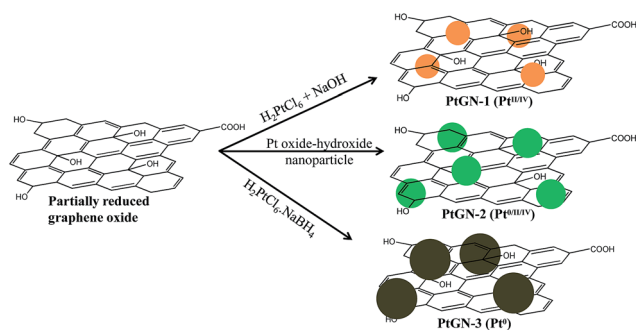
A glassy carbon electrode of 3 mm in diameter (surface area of 0.07 cm²) was carefully polished with 1, 0.3, and 0.05 μm alumina powder, sequentially, until a mirror finish was obtained. Next, the electrode was ultrasonically cleaned with ethanol and deionized water and dried in air at room temperature. Then the electrode was immersed in 0.5 M H₂SO₄ and was voltammetrically scanned from –0.4 to 1.2 V (*vs.* Ag/AgCl) at

a rate of 100 mV s^{-1} to clean the surface. Finally, the composite dispersion was dropped onto the GCE surface, dried in air at room temperature for 2 h and used for electrochemical measurements. The loading of Pt in PtGN-1/2/3 modified GCE were $2.2 \mu\text{g}$, $5.2 \mu\text{g}$ and $7.5 \mu\text{g}$, respectively. Electrochemical measurements were performed with a CHI633D Electrochemical Analyzer. A conventional three-electrode system was used for all electrochemical experiments, which consisted of a platinum wire as auxiliary electrode, an Ag/AgCl/saturated KCl as reference electrode and modified glassy carbon as working electrode. All experiments were conducted at room temperature. For the electro-oxidation of methanol, the cyclic voltammograms were recorded at a sweep rate of 50 mV s^{-1} in a mixture of H_2SO_4 (0.5 M) and methanol (1 M). All the current were normalized with the loading amount of catalyst in the electrode.

3. Results and discussion

3.1 Synthesis and characterization of platinum-graphene nanocomposite (PtGN)

We have focused on three different Pt-graphene nanocomposites designated as PtGN-1, PtGN-2 and PtGN-3 as shown in Scheme 1. The synthetic procedure for three composites and details of their characterization are shown in Scheme 1, Fig. 1 and 2, Table 1 and ESI, Fig. S1–S7.† Colloidal graphene oxide is synthesized by Hummer's method and then transformed into partially reduced graphene oxide *via* hydrazine reduction.^{21,29} Reaction of partially reduced graphene oxide with the basic solution of platinum salt produces PtGN-1. Platinum salt is transformed into colloidal platinum oxide by incubating in basic solution for 1–2 days and then reacted with partially reduced graphene oxide in preparing PtGN-2. Platinum salt is reduced by NaBH_4 in presence of partially reduced graphene oxide that produces PtGN-3. All the nanocomposites are isolated as solid by centrifugation and redispersed in fresh water *via* sonication. The colloidal form of nanocomposites is used as stock solution for their deposition on electrode surface.



Scheme 1 Schematic representation of synthesis steps for three different platinum nanoparticle-graphene nanocomposites. Partially reduced graphene oxide is reacted with platinum salt for preparation of PtGN-1, partially reduced graphene oxide is reacted with colloidal platinum oxide for preparation of PtGN-2 and platinum salt is reduced by NaBH_4 in presence of partially reduced graphene oxide for the preparation of PtGN-3.

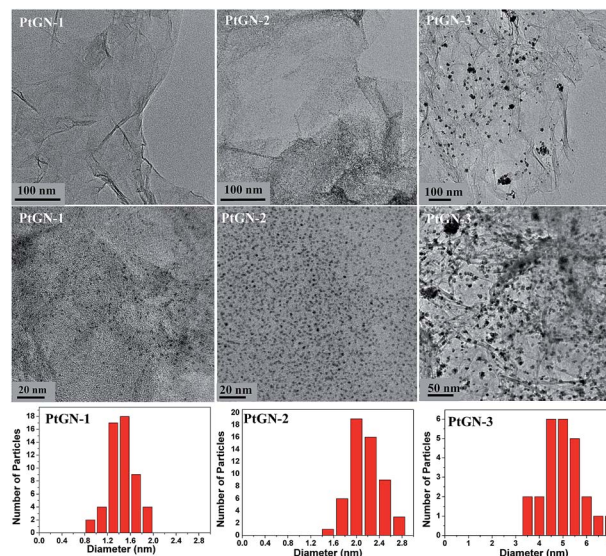


Fig. 1 TEM image at different magnifications and corresponding size distribution histograms of three nanocomposites. Average sizes of nanoparticles are 1.5 nm, 2.2 nm and 5.1 nm for PtGN-1, PtGN-2 and PtGN-3, respectively.

We have extensively investigated the size of platinum-based nanoparticles present on each nanocomposite. Fig. 1 and ESI, Fig. S1–S5† shows the TEM image of nanocomposites. Graphene flakes are clearly observed with uniformly distributed platinum nanoparticles, particularly for PtGN-1 and PtGN-2. However, nanoparticles present in PtGN-3 are observed with severe aggregation and distribution of nanoparticle are relatively less uniform. High resolution TEM image shows that there is a clear difference in nanoparticle size in three nanocomposites. The average sizes of nanoparticles are 1.5 nm, 2.2 nm and 5.1 nm for PtGN-1, PtGN-2 and PtGN-3, respectively. Other two PtGN with Pt nanoparticle of 0.95 nm and 2.0 nm has also been synthesized using the condition similar to PtGN-1.

X-ray photoelectron spectra (XPS) of PtGN-1 have been measured to investigate the chemical signature and oxidation state of Pt and carbon (Fig. 2 and ESI, Fig. S6 and S7†). Two oxidation states of Pt are observed in the deconvoluted Pt 4f

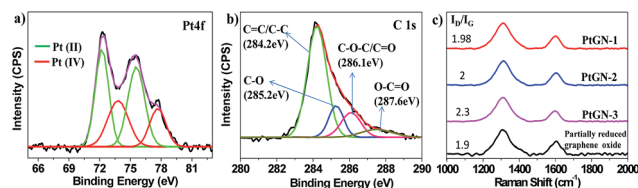


Fig. 2 (a) XPS characterization of PtGN-1 showing that platinum nanoparticles consist of Pt^{II} and Pt^{IV} . Deconvoluted Pt 4f spectrum displays four fitted signals at 72.2 eV ($\text{Pt } 4f_{7/2}$) and 75.5 eV ($\text{Pt } 4f_{5/2}$) corresponding to Pt^{IV} , and 73.4 eV ($\text{Pt } 4f_{7/2}$) and 77.7 eV ($\text{Pt } 4f_{5/2}$) attributed to Pt^{II} , (b) XPS characterization of C 1s of PtGN-1 showing signature of different types of carbon and (c) Raman spectra of PtGN-1, PtGN-2, PtGN-3 and partially reduced graphene oxide showing the defective bands at 1300 cm^{-1} and graphitic bands at 1600 cm^{-1} and the respective intensity ratio (I_D/I_G value).

Table 1 Property of three different nanocomposites used in this study (I_f/I_b represents ratio of forward to backward current intensity)

Samples	Pt loading (wt%)	Pt oxidation states	Electrochemical surface area ($\text{m}^2 \text{g}^{-1}$)	Forward peak position	I_f/I_b at 15 th and 105 th cycle
PtGN-1	10.9	Pt ^{II} (63%), Pt ^{IV} (37%)	22	0.56 V	1.87, 1.6
PtGN-2	22.5	Pt ⁰ (62%), Pt ^{II} (22%), Pt ^{IV} (16%)	64	0.69 V	0.87, 0.79
PtGN-3	25	Pt ⁰ (100%)	32	0.64 V	0.75, 0.81

spectra. The most intense doublet peaks at 72.2 eV (Pt 4f_{7/2}) and 75.5 eV (Pt 4f_{5/2}) are attributed to the Pt^{II} and other lower intense doublet peaks at 73.8 eV (Pt 4f_{7/2}) and 77.7 eV (Pt 4f_{5/2}) are attributed to the Pt^{IV} species.³² The relative percentage of Pt^{II} and Pt^{IV} are calculated from the peak areas which are 63% and 37%, respectively. The deconvoluted C 1s spectra of PtGN-1 shows signature corresponding to C=C/C-C, C-O, C-O-C/C=O and O-C=O groups with respective peaks at 284.2 eV, 285.2 eV, 286.1 eV and 287.6 eV, respectively.³³ Our earlier XPS study shows that PtGN-2 contain mixture of Pt (0), Pt (II), Pt (IV) and PtGN-3 contain Pt (0) only.²¹ The oxidation states of all the composites are summarized in Table 1.

The Raman spectra of composite displays G band at 1600 cm⁻¹ corresponding to the sp² hybridized carbon atoms and the D band at 1310 cm⁻¹ corresponding to disruption of the sp² hybridized carbon atoms. (Fig. 2) The intensity ratios of D band to G band (I_D/I_G) for different composites lies between 1.98–2.3, which are little larger than 1.9 corresponding to partially reduced graphene oxide. This suggests the increased defects in graphene structure after incorporation of metal nanoparticle.^{34,35}

3.2 Size and oxidation state effect of Pt on electrochemical performance

Electrochemical oxidation of methanol in H₂SO₄ media has been used to study the electrocatalytic performance of three different composites. Cyclic voltammetry (CV) has been used to systematically study the catalytic activity and onset potential of methanol oxidation. (Fig. 3 and 4 and ESI Fig. S8 and S9†) Two typical oxidation peaks appear on the CV for all the catalyst, arising due to the oxidation of methanol and its intermediates. The forward scan shows a peak in the range of 0.5–0.7 V which corresponds to oxidation of adsorbed methanol to metal

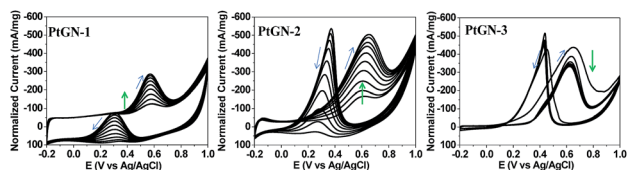


Fig. 3 First 10 electrochemical potential cycles towards 1 M methanol oxidation by three different nanocomposites. In each case glassy carbon electrode is modified with nanocomposites and then oxidation of 1 M methanol in 0.5 M H₂SO₄ is performed at a scan rate of 50 mV s⁻¹. The current density shown in the CVs are normalized by the respective mass of Pt loading.

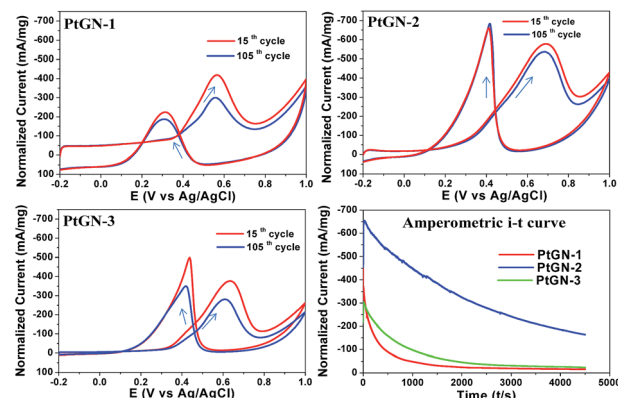


Fig. 4 (a–c) Electrocatalytic oxidation of methanol by PtGN-1, PtGN-2 and PtGN-3 nanocomposites, respectively. In each case glassy carbon electrode is modified with nanocomposites and then oxidation of 1 M methanol in 0.5 M H₂SO₄ is performed at a scan rate of 50 mV s⁻¹. The current density shown in the CVs is normalized by the respective mass of Pt loading. (d) Amperometric *i-t* study for comparing the stability of three catalysts in 1 M methanol and 0.5 M H₂SO₄ at 0.5 V.

carbonyl that involves removal of four electrons. The backward scan shows a peak in the range of 0.3–0.4 V which corresponds to the oxidation of adsorbed CO to CO₂ that makes the catalyst free from CO poisoning. This result indicates that catalytic methanol oxidation by all nanocomposites follow CO poisoning pathway and electrochemical reactions can be summarized in following two equations (Scheme 2).^{36,37}

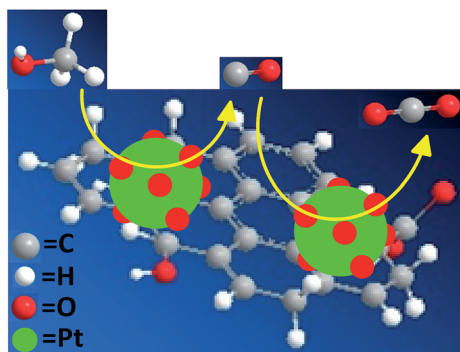
Anodic reaction:



Cathodic reaction:



Successive CV for first 10 cycles has been shown for three composites. (Fig. 3) In the case of PtGN-1 and PtGN-2, the forward and backward peak gradually becomes intense with increasing cycles. These results indicate the active catalyst in the form of Pt (0) is generated during electrochemical cycles and becomes stabilized. However, in the case of PtGN-3 those peaks are intense from the first cycle, suggesting that catalytically active Pt (0) is present from the first cycle. This observation is corroborated with oxidation state of Pt nanoparticle in three composites. (Table 1) Electrochemical surface area has been measured



Scheme 2 Mechanism of methanol oxidation by Pt-graphene nanocomposite.

for three catalysts and is highest for PtGN-2 (ESI, Fig. S9†) This result indicates that PtGN-2 provides most accessible active sites. This has been manifested from CV with the current densities normalized against loading of Pt. (Fig. 4a–c) The current density is highest for PtGN-2 and relatively stable after repeated cycles as compared to other two catalysts. The CO poisoning tolerance, measured by the ratio of forward to backward peak current, is significantly higher for PtGN-1 as compared to other two catalysts. For example, the ratio of forward to backward peak current is 1.87 for PtGN-1 but the values are 0.87 and 0.75 for PtGN-2 and PtGN-3, respectively. This tolerance of CO poisoning decreases with repeated electrochemical cycles and the change of values from 15th cycle to 105th cycle for each nanocomposites shows that the effect is most prominent for PtGN-1. (Table 1) Amperometric *i*-*t* study has been performed for three composites for the evaluation of catalyst stability. (Fig. 4d) The current density shows most rapid decay for PtGN-1 during the initial period but for other two composites the decay is slow. This result indicates that deactivation of PtGN-1 is faster than other two composites.

Thus electrocatalytic methanol oxidation shows five significant differences between three nanocomposites which are due to the effect of Pt nanoparticle size and oxidation state. First, catalytic current increases with increasing electrochemical cycle for PtGN-1 and PtGN-2, but for PtGN-3 catalytic current is high from beginning. This is because the active catalyst in the form of Pt (0) is generated during electrochemical cycles in the case of PtGN-1 and PtGN-2, but for PtGN-3 the active Pt (0) is already present. Second, the forward oxidation peak of methanol is lowest for PtGN-1 (0.56 V) but for other two composites the values are very similar. (0.67 V and 0.64 V) which suggests that anodic methanol oxidation is easier at PtGN-1 surface compared to other composites. Third, CO poisoning tolerance is significantly higher for PtGN-1 as compared to other two catalysts but this tolerance decreases with repeated electrochemical cycles and the effect is most prominent for PtGN-1. This suggests that the advantage of high CO poisoning tolerance by PtGN-1 is lost rapidly during electro-catalysis. Fourth, electrochemical surface area and normalized catalytic current are highest for PtGN-2 as compared to PtGN-1 and PtGN-3. This suggests that PtGN-2 offers most accessible active sites with best overall catalytic performance. Fifth, among all the catalysts the

PtGN-2 offers high and stable current with best catalyst durability.

The differential electrocatalytic performance by three catalysts can be explained based on the size and oxidation states of platinum nanoparticle. The well-known mechanism of methanol electro-oxidation in acidic media involves CO intermediate as shown in eqn (1) and (2). Platinum nanoparticles present in PtGN-1 and PtGN-2 are composed of mixed valence states and active Pt (0) sites are surrounded with oxygen of Pt (II) and Pt (IV). (Scheme 2) These oxygenic platinum offers stable grafting with graphene surface, prevents destruction of active Pt (0) sites and facilitate conversion of CO to CO₂.³⁸ Lower onset potential and lower CO poisoning by PtGN-1 is linked to the smallest size of nanoparticle. However, as the reaction progress, these advantages are lost due to gradual decrease of active Pt (0) sites formed during first 10 cycles by the formation of irreversible oxide layer which prevent the oxidation of methanol and increase of nanoparticle size.³⁹ Poorest catalytic activity of PtGN-3 can be explained due to largest size of nanoparticles, severe aggregation between nanoparticles and presence of exclusive Pt (0) which is highly prone to attack by CO species. All these results can explain the 2.2 nm Pt with mixed oxidation state as the optimum size for best electrocatalytic performance. This size offers moderate onset potential of methanol oxidation with lower CO tolerance and the active Pt (0) is best stabilized. Further lowering of size can offer methanol oxidation at low over-potential and with high CO tolerance but the catalytic activity and current stability is compromised. Poor performance by larger size Pt is due to higher over-potential of methanol oxidation, lower CO tolerance, low accessibility of active sites and poor current stability.

4. Conclusion

In summary, we have synthesized graphene-based composite with platinum nanoparticles where the size of nanoparticle varies from 1 to 5 nm with different oxidation states of metal and test their catalytic activity towards methanol electro-oxidation. We found that 2.2 nm platinum nanoparticle with mixed oxidation state offers best overall electro-catalytic performance. This optimum size requirement can be explained by effect of platinum nanoparticle size on methanol oxidation over-potential, CO poisoning tolerance and catalyst stability under repeated electrochemical cycle. Although the smaller size offers low over-potential methanol oxidation and high CO tolerance, the catalytic current rapidly decays with repeated cycle. Poor performance by larger size Pt is due to increased over-potential of methanol oxidation, lower CO tolerance, low accessibility of active sites and poor current stability. In the optimum size of 2.2 nm the advantages of smaller size is partially compromised but accessibility of active sites and catalyst stability are compensate them. Mixed valence oxygenic Pt offers better CO tolerance and long term catalyst stability. This understanding of nanoparticle size effect would offer in the design of electrocatalyst with better performance.

Acknowledgements

NRJ would like to thank DST, government of India for financial assistance. AM acknowledges CSIR, India for providing research fellowship.

Notes and references

- 1 C. Huang, C. Li and G. Shi, *Environ. Sci.*, 2012, **5**, 8848–8868.
- 2 S. K. Bhunia and N. R. Jana, *ACS Appl. Mater. Interfaces*, 2014, **6**, 20085–20092.
- 3 G. M. Scheuermann, L. Rumi, P. Steurer, W. Bannwarth and R. Mulhaupt, *J. Am. Chem. Soc.*, 2009, **131**, 8262–8270.
- 4 X. Huang, Z. Zhao, J. Fan, Y. Tan and N. Zheng, *J. Am. Chem. Soc.*, 2011, **133**, 4718–4721.
- 5 C. V. Rao, C. R. Cabrera and Y. Ishikawa, *J. Phys. Chem. C*, 2011, **115**, 21963–21970.
- 6 X. Chen, G. Wu, J. Chen, X. Chen, Z. Xie and X. Wang, *J. Am. Chem. Soc.*, 2011, **133**, 3693–3695.
- 7 S. Guo, S. Dong and E. Wang, *ACS Nano*, 2010, **4**, 547–555.
- 8 H. Yin, H. Tang, D. Wang, Y. Gao and Z. Tang, *ACS Nano*, 2012, **6**, 8288–8297.
- 9 J. Hou, Y. Shao, M. W. Ellis, R. B. Moore and B. Yi, *Phys. Chem. Chem. Phys.*, 2011, **13**, 15384–15402.
- 10 S. Guo, D. Wen, Y. Zhai, S. Dong and E. Wang, *ACS Nano*, 2010, **7**, 3959–3968.
- 11 Z. Sun, J. Masa, W. Xia, D. Konig, A. Ludwig, Z. A. Li, M. Farle, W. Schuhmann and M. Muhler, *ACS Catal.*, 2012, **2**, 1647–1653.
- 12 S. Sharma, A. Ganguly, P. Papakonstantinou, X. Miao, M. Li, J. L. Hutchison, M. Delichatsios and S. Ukleja, *J. Phys. Chem. C*, 2010, **114**, 19459–19466.
- 13 D. Li, C. Wang, D. Tripkovic, S. Sun, N. M. Markovic and V. R. Stamenkovic, *ACS Catal.*, 2012, **2**, 1358–1362.
- 14 C. Xu, X. Wang and J. Zhu, *J. Phys. Chem. C*, 2008, **112**, 19841–19845.
- 15 H. W. Ha, I. Y. Kim, S. J. Hwang and R. S. Ruoff, *Electrochem. Solid-State Lett.*, 2011, **14**, B70–B73.
- 16 P. Kundu, C. Nethravathi, P. A. Deshpande, M. Rajamathi, G. Madras and N. Ravishankar, *Chem. Mater.*, 2011, **23**, 2772–2780.
- 17 Y. J. Wang, D. P. Wilkinson and J. Zhang, *Chem. Rev.*, 2011, **111**, 7625–7651.
- 18 S. Zhang, Y. Shao, H. Liao, J. Liu, I. A. Aksay, G. Yin and Y. Lin, *Chem. Mater.*, 2011, **23**, 1079–1081.
- 19 S. Zhang, Y. Shao, H. Liao, M. H. Engelhard, G. Yin and Y. Lin, *ACS Nano*, 2011, **5**, 1785–1791.
- 20 J. D. Qiu, G. C. Wang, R. P. Liang, X. H. Xia and H. W. Yu, *J. Phys. Chem. C*, 2011, **115**, 15639–15645.
- 21 A. Mondal and N. R. Jana, *ACS Catal.*, 2014, **4**, 593–599.
- 22 Y. Li, W. Gao, L. Ci, C. Wang and P. M. Ajayan, *Carbon*, 2010, **48**, 1124–1130.
- 23 S. Sun, G. Zhang, N. Gauquelin, N. Chen, J. Zhou, S. Yang, W. Chen, X. Meng, D. Geng, M. N. Banis, R. Li, S. Ye, S. Knights, G. A. Botton, T. K. Sham and X. Sun, *Sci. Rep.*, 2013, **3**, 1–9.
- 24 Y. Shen, Z. Zhang, R. Long, K. Xiao and J. Xi, *ACS Appl. Mater. Interfaces*, 2014, **6**, 15162–15170.
- 25 C. Cremers, M. Scholz, W. Seliger, A. Racz, W. Knechtel, J. Rittmayr, F. Grafwallner, H. Peller and U. Stimming, *Fuel Cells*, 2007, **7**, 21–31.
- 26 C. Coutanceau, R. K. Koffi, J. M. Leger, K. Marestin, R. Mercier, C. Nayoze and P. Capron, *J. Power Sources*, 2006, **160**, 334–339.
- 27 Y. Qiao and C. Li, *J. Mater. Chem.*, 2011, **21**, 4027–4036.
- 28 D. S. Cameron, G. A. Hards, B. Harrison and R. J. Potter, *Platinum Met. Rev.*, 1987, **31**, 173–181.
- 29 A. Mondal, A. Sinha, A. Saha and N. R. Jana, *Chem.–Asian J.*, 2012, **7**, 2931–2936.
- 30 M. T. Reetz and M. G. Koch, *J. Am. Chem. Soc.*, 1999, **121**, 7933–7934.
- 31 M. R. Gao, Z. Y. Lin, J. Jiang, C. H. Cui, Y. R. Zheng and S. H. Yu, *Chem.–Eur. J.*, 2012, **18**, 8423–8429.
- 32 J. F. Moulder, F. W. Stickle, P. E. Sobol and K. D. Bomben, *Perkin-Elmer*, 1995.
- 33 C. Mattevi, G. Eda, S. Agnoli, S. Miller, K. A. Mkhoyan, O. Celik, D. Mastrogiovanni, G. Granozzi, E. Garfunkel and M. Chhowalla, *Adv. Funct. Mater.*, 2009, **19**, 2577–2583.
- 34 K. S. Subrahmanyam, A. K. Manna, K. Pati Swapan and C. N. R. Rao, *Chem. Phys. Lett.*, 2010, **497**, 70–75.
- 35 X. Liu, C. Meng and Y. Han, *J. Phys. Chem. C*, 2013, **117**, 1350–1357.
- 36 S. K. Meher and G. R. Rao, *ACS Catal.*, 2012, **2**, 2795–2809.
- 37 Y. X. Chen, A. Miki, S. Ye, H. Sakai and M. Osawa, *J. Am. Chem. Soc.*, 2003, **125**, 3680–3681.
- 38 L. R. Merte, M. Ahmadi, F. Behafarid, L. K. Ono, E. Lira, J. Matos, L. Li, J. C. Yang and B. R. Cuenya, *ACS Catal.*, 2013, **3**, 1460–1468.
- 39 J. W. Nicoletti and G. M. Whitesides, *J. Phys. Chem.*, 1989, **93**, 759.